The Mechanism of Char Ignition in Fluidized Bed Combustors

ROLAND V. SIEMONS

Department of Chemical Technology, University of Twente, Enschede, The Netherlands*

Knowledge about ignition processes of coal in fluidized beds is of importance for the start-up and dynamic control of these combustors. Initial experiments in a transparent fluidized bed scale model showed the existence of a considerable induction period for the ignition of char, especially at low bed temperatures (e.g., 800-950K for bituminous coal). This paper focuses on char-ignition delay at these low temperatures. It is shown that temperature rise during ignition is not caused by coal particle diameter shrinkage but rather by an increase in reactivity. Analysis of the thermal ignition process leads to the conclusion that the process is noncritical, causing a gradual temperature rise without Semenov Jump. Consequences of this result for future research are expounded. Calculated values of the maximum inclination of the heat generation curve (heat release versus coal particle temperature) may be of use to the development of an adequate experimental device.

1. INTRODUCTION

After a coal particle is introduced in a fluidized bed combustor it needs some time to reach a stable temperature which is high enough above the bed temperature for maintaining a steady operation mode of the combustor. We call this period "char-ignition delay." (The distinction between ignition of char and of volatiles is briefly discussed below). Figure 1 shows the char-ignition delay as a function of bed temperature for cokes of a bituminous coal. (Data of this coal type are listed in Table 1.) This result is part of the research done by M. Radovanović et al. [1] at Twente University of Technology, which will be reported in due course [2]. Single coal particle ignition experiments were carried out in a two-dimensional transparent fluidized bed (15 × 200 × 125 mm³), constructed by W. Prins [2], which was electrically heated (Fig. 2). The fluidizing gas was a mixture of oxygen and nitrogen; the bed material consisted of 0.5 mm diam. alumina spheres. The construction made it

possible to observe the coal particle visually, both directly and by TV-video. Slow-motion and freeze-frame analyses were carried out. In these experiments char-ignition delay was roughly approached by measuring the time lag from the introduction of the char particle until the moment at which the coal particle started to glow visibly. Also presented in Fig. 1 are estimations of heating times for nonreacting coal particles to reach the bed temperature (see Appendix). It is clear that at low bed temperatures the ignition takes more time than the heating does. Apart from bed temperature, char-ignition delay depends strongly on coal type and oxygen mol-fraction .

The phenomenon of char-ignition delay has important implications for the start-up and dynamic control of fluidized bed combustors. Central questions are

1. Does a minimum bed temperature above which coal feeding can be started exist, and if so, what are its physical determinants?
2. How can a simple experimental method by which the ignition behavior in fluidized beds can be tested for various coal types and circumstances be designed?

---

* The research reported upon in this paper was carried out at the Department of Mechanical Engineering, University of Twente.
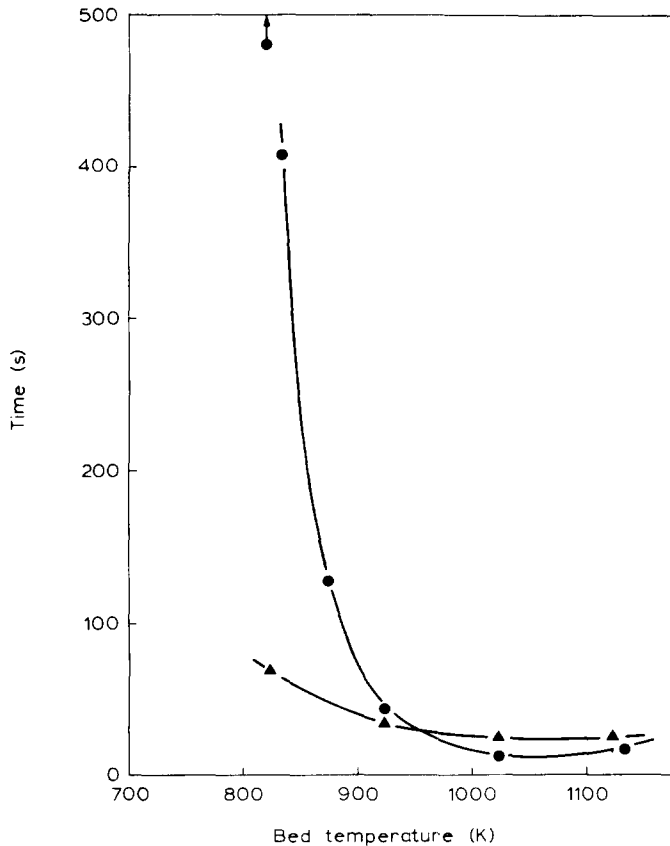
Fig. 1. Experimental data of char-ignition delay ($\bullet$) and estimated heating times ($\blacktriangle$) as a function of bed temperature ($\uparrow$: no ignition observed). $d = 8.6$ mm, $U_f = U_{mf} + 0.25$ m/s, $X_{O_2} = 0.21$.

TABLE 1

Analysis of a Bituminous Coal

Proximate (%)	
Moisture	1.9
Volatile matter	35.3
Ash	19.2
Fixed carbon (by difference)	43.6

Ultimate (%)	
Carbon	64.9
Hydrogen	3.4
Nitrogen	0.9
Sulfur	0.8
Oxygen	9.0
Chlorine	0.1

These questions can only be answered if we have a physical understanding of the char-ignition delay.

When coal is introduced into a fluidized bed combustor devolatilization occurs and volatiles ignition as well as char ignition may take place in the same time interval and thus influence each other. Devolatilization might cause a pressure gradient preventing oxygen transport to and into the coal particle. To what extent this contributes to char-ignition delay is not part of this study. The consumption of oxygen by burning volatiles is another possible reason for char-ignition delay. However for a lignite it has been established by Prins et. al. [2] that volatile matter will only ignite at bed temperatures above 950K. It may be expected that volatile matter evolved from higher rank coals will ignite only at even higher bed temperatures. Therefore, since we are interested
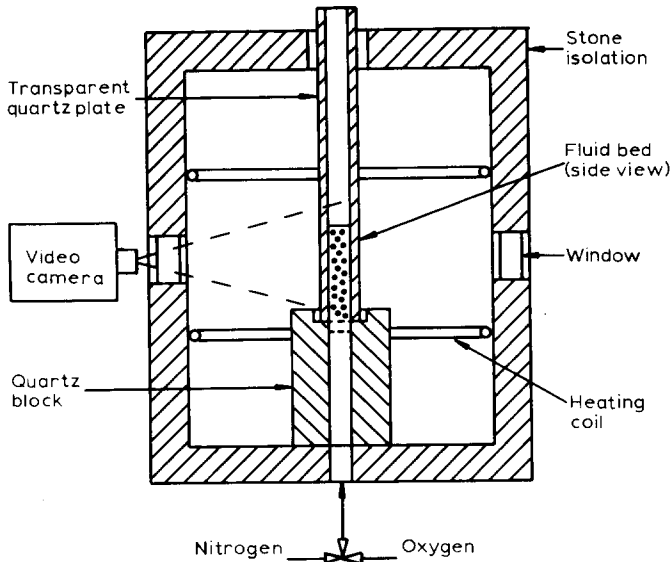
Fig. 2. Cross-sectional side view of the two-dimensional fluidized bed construction.

in the behavior at low bed temperatures, char ignition can be discussed independently of the ignition of volatile matter.

The study of ignition properties must be linked closely to the intended application of the fuel. Typical for fluidized bed combustion are uniform bed temperature and good heat transfer between the bed and inserted surfaces. Essenhigh [4] gives an extended review of the position of ignition research. But he does not mention any study concerning the mechanism of char ignition in fluidized beds.

2. STATEMENT OF THE PROBLEM

The char-ignition process is controlled by three almost independent characteristics: thermal inertia of the char particle, heat generation by combustion, and heat transfer between the char particle and the surrounding bed. They lead to the following equation (see list of symbols for meanings):

$$mC_p\, \partial T/\partial t = Q_g - Q_t. \tag{1}$$

If carbon is converted partially to CO and partially to CO_2 we may write for Q_g,

$$Q_g = [H_{CO_2}\Lambda_{CO_2}/M_{CO_2}) + (H_{CO}\Lambda_{CO}/M_{CO})$$
$$- (h_{char} - h_{graphite})]\dot{m}_C$$
$$= (H_r/M_C)\dot{m}_C, \tag{2}$$

where H_j is the enthalpy of formation of species j

from the elements and Λ_j is a gravimetric conversion coefficient, denoting the ratio of the mass flow of species j and the total carbon mass flow $\dot{m}_C$. H_r is the enthalpy of the actual reaction per mole of carbon. The term $(h_{char} - h_{graphite})$ is included since the enthalpy of formation of CO and CO_2 is defined with reference to graphite instead of char. Its value can be measured by comparing the heat release of combusting graphite and char at a constant temperature. In this paper, however, it will be neglected.

If heat generation and transfer are plotted as a function of temperature the heat generation curve takes the shape of an S, owing to its dependence on both chemical kinetics and mass transfer, while the curve of heat transfer is almost a straight line. (Radiation plays only a minor role—see Section 3.) At their point of intersection, $\partial T/\partial t = 0$. This point defines the overtemperature of the char particle (see Fig. 3). At the right-hand branch of the S-curve combustion is principally controlled by external oxygen transport, at the left-hand branch by chemical kinetics and intraparticle oxygen diffusion. Traditionally, only char particles that burn in the external oxygen transport regime are said to be ignited.

Most studies of the transition from the kinetic and pore diffusion controlled regime to the external transport regime, thus assessing ignition tem-
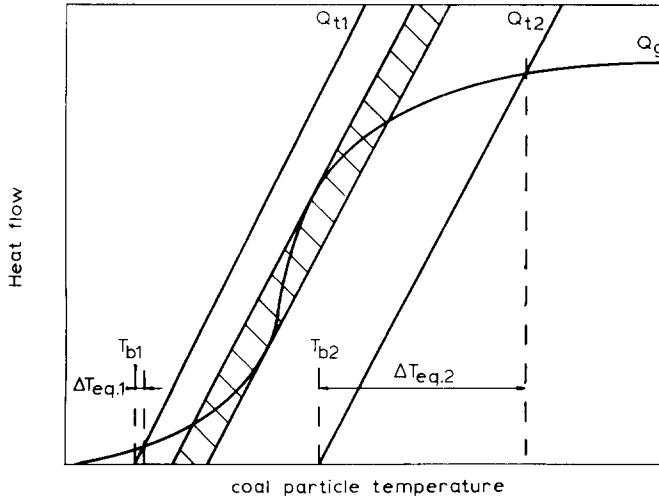
Fig. 3. Determination of the char particle overtemperature ΔT_{eq} by the char particle's heat generation and heat transfer from the char particle to the fluidized bed. Situations at low (1) and high (2) bed temperature, respectively. Shaded area: bistable region.

perature and delay, are limited to the evaluation of the "Tangency Criterion" which defines unstable points by $Q_g = Q_t$ and $\partial Q_g/\partial T = \partial Q_t/\partial T$. Naturally, such analysis is only possible for those devices where these points may exist, i.e., if the maximum inclination of the heat generation curve is steeper than the curve of heat transfer. After Vulis [5] we call this condition critical, whereas we call the other case, where unstable points do not exist, noncritical.

The difference between the two ignition modes has great consequences for the measurableness of ignition delay. Ignition delay, markedly exceeding the time required for the char particle to reach the bed temperature, must be due to relative changes between heat generation and transfer. The transformations conceivable with fluidized bed combustion are shown in Fig. 4. In case of critical conditions, while passing through an unstable point, the equilibrium char particle temperature
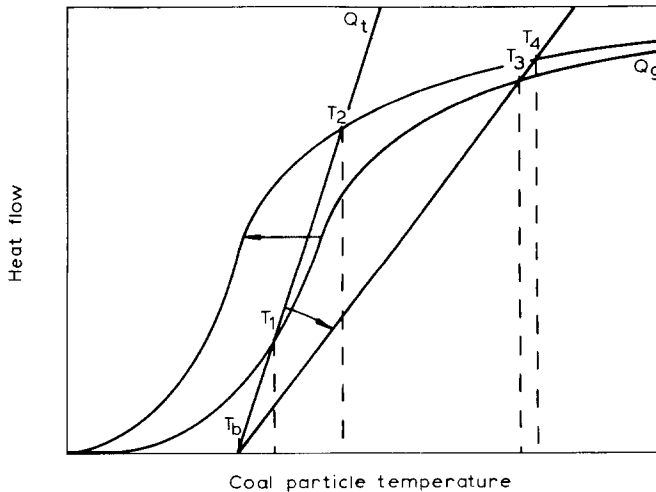

Fig. 4. Possible changes of heat generation and heat transfer for an igniting char particle in a fluidized bed. T_1; char particle equilibrium temperature at $t = 0$; T_2; same after change of heat generation rate; T_3; same after change of heat transfer rate; T_4; same after combined change of heat generation and transfer rate.
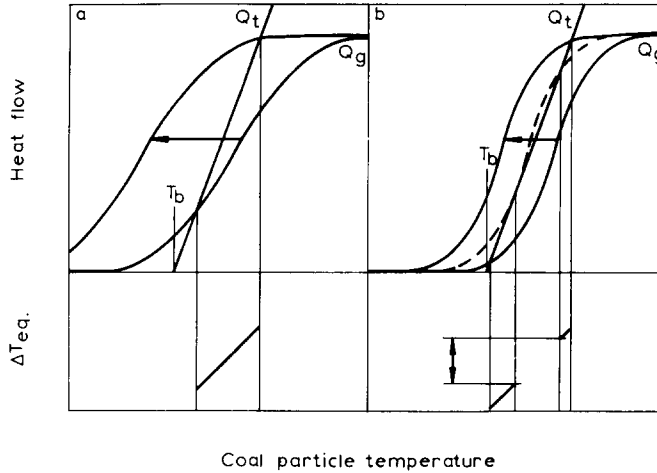
Fig. 5. Two ignition modes. Noncritical (a) with continuous and critical (b) with discontinuous rising equilibrium char particle overtemperature, ΔT_{eq}.

changes discontinuously, thus causing a rapid temperature rise, the so-called Semenov Jump. Otherwise this jump will be absent with only a slow temperature change, (Fig. 5).

In this paper an attempt is made to answer two questions:

1. What are the physical properties that cause the changing relation between heat generation and heat transfer?
2. Are ignition conditions in fluidized bed combustors critical or noncritical?

We shall not immediately look for solutions to the unsteady-state equation [Eq. (1)], but rather investigate its quality.

3. METHOD

To evaluate these matters the inflection point of the heat generation curve, i.e., its temperature T^* and inclination $(\partial Q_g/\partial T)^*$, will be determined and compared to the position of the heat transfer curve. We shall look especially for the influence of char particle diameter, oxygen mol-fraction, and reactivity, the latter defined on actual mass base as

$$R_m = A \exp(-E/RT) \ C^m.$$

The starting point of heat generation analysis is a conversion model for a spherical char particle, taking account of both external and internal oxygen transport as well as of the simultaneous conversion of oxygen within the particle. Thus, effects of pyrolysis and devolatilization are neglected. We shall assume that during ignition there is no ash layer and that the char particle is isothermal (see Appendix). Further, we assume that the char particle is homogeneous with respect to density, reactivity, and effective diffusivity at the moment it has attained the bed temperature. The equations derived in this section are meant for this point of time.

The mass balance for a spherical layer within the char particle reads

$$4\pi r^2 \ \partial r \ \rho \Lambda_{O_2} A \ \exp(-E/RT) \ C^m$$

$$= 4\pi \ \partial r \ \frac{\partial}{\partial r} \left(r^2 D_e \ \frac{\partial C}{\partial r} \right) - 4\pi r^2 \ \partial r \ \frac{\partial C}{\partial t} \ , \quad (3)$$

with the boundary conditions

$$r = 0: \quad \partial C/\partial r = 0, \qquad C = C_c$$

and

$$r = d/2: \quad \partial C/\partial r = (k/D_e)(C_b - C_s), \qquad C = C_s.$$

In Eq. (3) the oxygen gravimetric conversion coefficient depends on the ratio of CO and CO_2 production z,

$$\Lambda_{O_2} = (M_{O_2}/M_C)(z/2 + 1)/(z + 1). \quad (4)$$

Integration of Eq. (3) yields the carbon mass flux

$$\dot{m}_C = (4\pi/\Lambda_{O_2}) \int_0^{d/2} \left[\frac{\partial}{\partial r}\left(r^2 D_e \frac{\partial C}{\partial r} \right) - r^2 \frac{\partial C}{\partial t} \right] \partial r,$$

(5a)

$$\dot{m}_C = 4\pi\rho A \, \exp(-E/RT) \int_0^{d/2} r^2 C^m \, \partial r.$$ (5b)

If the regime is quasi-stationary,

$$\frac{\partial C}{\partial t} \ll \frac{1}{r^2}\frac{\partial}{\partial r}\left(r^2 D_e \frac{\partial C}{\partial r} \right),$$

then, making use of the boundary conditions, we may write Eq. (5a) as

$$\dot{m}_C = \pi d^2 k(C_b - C_s)/\Lambda_{O_2}.$$ (6a)

The assumption is allowed in the stable combustion region, certainly if the ignition process turns out to be noncritical (see Appendix). Defining the effectiveness factor η as η = actual conversion velocity/conversion velocity if $C(r) = C_s$, or, for homogeneous particles,

$$\eta = \int_0^{d/2} r^2 C^m \, \partial r/(d^3 C_s^{\,m}/24),$$ (7)

we find for Eq. (5b)

$$\dot{m}_C = \frac{1}{6}\,\pi d^3 \rho A \, \exp(-E/RT) \, C_s^{\,m}\eta.$$ (6b)

The solution to η as a function of the Thiele modulus ϕ is given by Aris [6, 7] and Mehta [7]. We define the Thiele modulus as

$$\phi = (d/2)[(m+1)\rho\Lambda_{O_2}A$$
$$\times \exp(-E/RT) \, C_s^{\,m-1}/(2D_e)]^{1/2}.$$ (8)

Refashioned for this definition the solution to the effectiveness factor reads [8]

$$\eta = (3/\phi)[(\phi - \tanh \phi)/\phi \tanh \phi].$$ (9)

From Eqs. (6) the surface oxygen concentration C_s can be eliminated, and the carbon mass flux and subsequently the heat generation [Eq. (2)] can be determined as a function of temperature.

Besides the independent parameters to be varied freely, values of mass transfer and the CO/CO_2-ratio must be estimated. An empirical correlation given by Prins et al. [9] is used to calculate values of external mass transfer. Independent parameters are bed particle and char particle diameters, minimum fluidization velocity, and bed porosity.

The effective internal diffusivity depends on both particle porosity and temperature. Empirically Bliek [10] has established that

$$D_e \sim \psi^3/2.5.$$

Taking account of both Knudsen and binary diffusion the temperature dependence is given by Leaurendeau [8]:

$$D_e \sim [(1/D_k) + (1/D_b)]^{-1},$$

and

$$D_k = (\delta/3)(8RT/\pi M)^{1/2}, \qquad D_b \sim T^{1.75}.$$

Since data for intraparticle diffusion at high temperatures are not at our disposal, we use these relations to extrapolate data obtained at room temperature.

The ratio of CO and CO_2 production is calculated from a correlation given by Arthur [11]. Other correlations are available, e.g., Rossber [12], but the influence of this parameter will turn out to be rather small.

In contrast with our discussion of the heat generation curve and of the data necessary for its determination, a less extended reflection suffices for the curve of heat transfer from the char particle to the surrounding bed. A review concerning this problem is given by Prins et al. [13]. An important implication of their experimental work is that radiation plays only a minor role up to temperatures of 1200K. They present a relation for the maximum Nusselt number, which allows evaluation of the diameter and temperature dependence. (Heat transfer depends on the fluidization velocity. Fluidized bed combustors are expected to operate in the regime where heat transfer between fuel and bed material is maximum—Prins et al. [13].) Thus we find for heat transfer

$$Q_t = (\mathrm{Nu}_{max} \, \lambda_g/d_b)\pi d^2(T - T_b).$$ (10)

In our laboratory the necessary data were measured for cokes of the bituminous coal and the small scale fluidized bed mentioned in Section 1. All data are summarized in Table 2.

4. AN ANALYTICAL SOLUTION

The curve of heat transfer is a straight line through the bed temperature with an inclination of

$$\partial Q_t / \partial T = \pi d^2 \text{ Nu } \lambda_g / d_b. \tag{11}$$

Determination of the heat generation inflection point is more problematic. It is analytically determined by $\partial^2 Q_g / \partial T^2 = 0$. We shall shall assume

that the reaction order $m = 1$ since we prefer analytical to numerical solutions. Then Eq. (6) reduces to

$$\dot{m}_C = \pi d^2 [\Lambda_{O_2}/k + 6/\eta d\rho A$$

$$\times \exp(-E/RT)]^{-1} C_b. \tag{12}$$

If the Thiele modulus $\phi > 15$, Eq. (9) can be approximated by $\eta = 3/\phi$. Making use of this relation Eq. (12) is transformed to

$$\dot{m}_C = \pi d^2 [\Lambda_{O_2}/k + (\Lambda_{O_2}/\rho D_e A)^{1/2}/$$

$$\exp(-E/2RT)]^{-1} C_b. \tag{13}$$

TABLE 2

Data Used[a]

Parameter	Value	Unit	Source
A	$48.7 \times 10^3 (K) T_b$	kg/m^3	
$D_b(O_2-N_2)$	9.71×10^{-10}	m^2/s	Refs. [8] and [19]
d_b	0.5×10^{-3}	m	
δ	350×10^{-10}	m	
E	141.5×10^6	J/kmol	
ϵ	0.4	—	
H_{CO}			Ref. [18]
H_{CO_2}			Ref. [18]
λ_g			Ref. [18]
m (reaction order)	1	—	
ν_g			Ref. [20]
ψ	0.365	—	
ρ_b	3800	kg/m^3	
ρ_c	1.1×10^3	kg/m^3	
U_{mf}	$17.01 T^{-0.646}$	m/s	
z	$10^{3.4} \exp(-51.8 \times 10^6 (J/kmol)/RT)$	—	Ref. [11]

[a] k from

$\epsilon_{mf} j_D \text{ Re}_{mf}{}^a = 0.105 + 1.505 (d/d_b)^{-1.05}$ (Ref. [9]),

$a = 0.35 + 0.29 (d/d_b)^{-0.50}$,

with

$j_D = (k/U_{mf})(\nu_g/D_b)^{2/3}$,

$\text{Re}_{mf} = U_{mf} d_d / [\nu_g (1 - \epsilon_{mf})]$.

Nu$_{max}$ from

$\text{Nu}_{max} = c \text{ Ar}^a$ (Ref. [13]),

$c = 3.539 (d/d_b)^{-0.257} (0.844 + 0.0756 T_b/273(K))$,
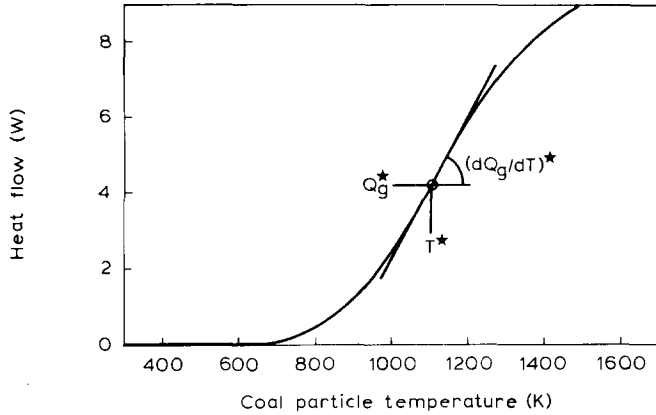
$a = 0.105 (d/d_b)^{0.082}$.

Fig. 6. Calculations of heat generation from the original equations [Eqs. (2), (9), (12)] and of the inflection point (*) from Eqs. (14).

It turns out that the inflection point is indeed found at temperatures for which $\phi > 15$, so that Eq. (13) proves to be a sound basis for the calculation of the heat generation [Eq. (2)]. Supposing that the logarithmic temperature dependence in Eq. (13) dominates the temperature dependence of the reaction enthalpy, the coefficient of mass transfer, and the oxygen gravimetric coefficient, the inflection point is found to be determined by the following implicit relations:

T^* by

$$[(E/R + 4T^*)/(E/R - 4T^*)] \exp(-E/2RT^*)$$
$$= (k^2/D_e\rho A \Lambda_{O_2})^{1/2}, \tag{14a}$$

Q_g^* by

$$Q_g^* = \pi d^2(k/\Lambda_{O_2})[(E/R - 4T^*)/(2E/R)]C_bH_r, \tag{14b}$$

and the inclination by

$$(\partial Q_g/\partial T)^* = \pi d^2(k/\Lambda_{O_2})[(E^2/R^2 - 16T^{*2})/$$
$$(8T^{*2}E/R)]C_bH_r. \tag{14c}$$

The dominance of the exponential temperature dependence was verified by calculating the original heat-generation curve from Eqs. (2), (9), and (12) and comparing this with the inflection point calculated from Eq. (14). The supposition is allowed, as illustrated by Fig. 6.

Explicit approximations for T^*, Q_g^*, and $(\partial Q_g/$

$\partial T)^*$ clarify the importance of the various parameters. They read

$$T^* \simeq (E/R)/\ln(\rho A \Lambda_{O_2} D_e/k^2), \tag{15a}$$

$$Q_g^* \simeq \tfrac{1}{2} \pi d^2(k/\Lambda_{O_2})C_bH_r \tag{15b}$$

(which is half of the heat generated if the char particle burns while limited by external mass transfer), and

$$(\partial Q_g/\partial T)^* \simeq \tfrac{1}{8} \pi d^2(k/\Lambda_{O_2})(R/E)$$
$$\times [\ln(\rho A \Lambda_{O_2} D_e/k^2)]^2 C_bH_r \tag{15c}$$

$$\simeq \tfrac{1}{8} \pi d^2(k/\Lambda_{O_2})(E/RT^{*2})C_bH_r. \tag{15d}$$

We see that the activation energy is directly proportional to the inflection point temperature, while inversely proportional to the maximum inclination of the heat generation curve. The oxygen mol-fraction is proportional to the maximum inclination. The influence of particle dimensions is expressed in the coefficient of external mass transfer.

5. RESULTS

The questions raised in Section 2 will be discussed here successively. Figures 7–10 show the results of calculations concerning heat generation [Eqs.
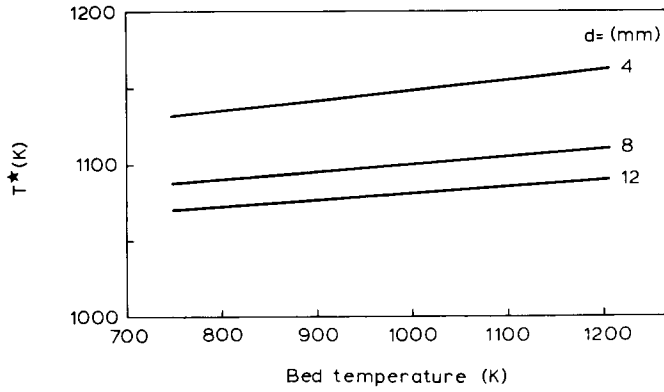
Fig. 7. Inflection point temperature as a function of bed temperature for 3 char particle diameters. $X_{O_2} = 0.21$.
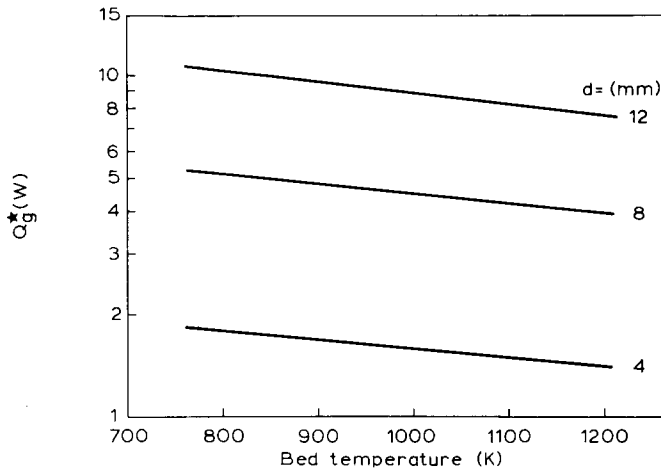
Fig. 8. Inflection point heat generation as a function of bed temperature for 3 char particle diameters. $X_{O_2} = 0.21$.
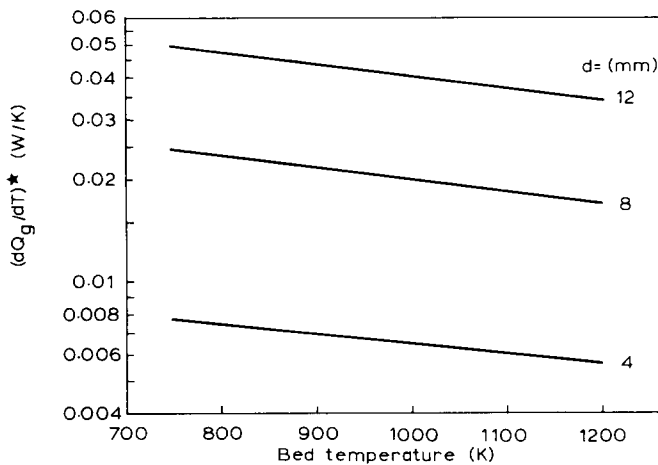
Fig. 9. Inflection point inclination as a function of bed temperature for 3 char particle diameters. $X_{O_2} = 0.21$.
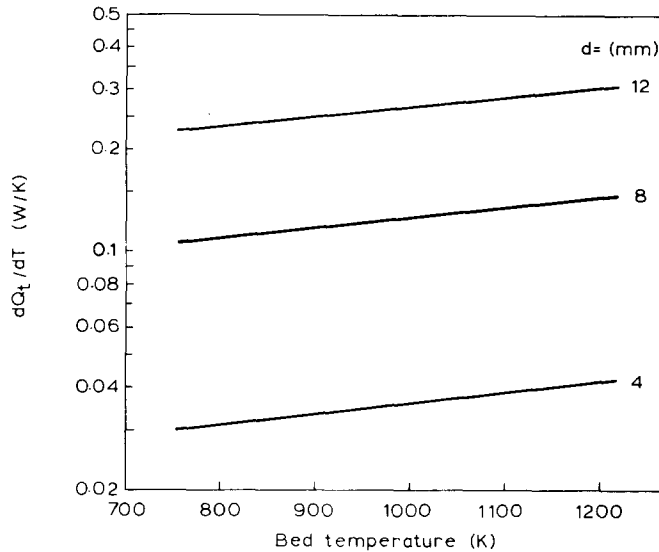
Fig. 10. Inclination of the heat transfer curve as a function of bed temperature for 3 char particle diameters. $X_{O_2} = 0.21$.

(14)] as well as heat transfer [Eq. (11)], as a function of bed temperature for 3 different char particle diameters. Assuming that the reaction order $m = 1$ these calculations are valid in a first period after introduction of the char particle into the fluidized bed, as long as conversion has not caused serious inhomogeneities. The inflection point temperature lies between 1075 and 1160K. For bed temperatures below 1050–1110K, depending on char particle size, this means that in the first instance char particles will burn at relatively low temperatures in the kinetic and pore diffusion controlled regime. Nonetheless experiments at lower bed temperatures indicate a considerable char particle overtemperature after an induction period up to 400 s (see Fig. 1).

The reason for this remarkable fact might be decrease of heat transfer (see Fig. 4) caused by diameter shrinkage of the burning char particle. However, the heat generation inflection point of smaller char particles is situated at higher temperatures (see Fig. 7), so this cannot explain properly the phenomenon of ignition delay. Therefore, since the reason cannot be found in heat transfer, the heat generation inflection point must shift to lower temperatures as indicated in Fig. 11. We can imagine how this comes about. In a first period conversion leads to an increase of the char

particle's internal surface area, and consequently to an increase of both the preexponential reactivity constant A and the effective diffusivity D_e [8]. For uniformly burning char particles, Eq. (15a) indicates how these parameters determine the decrease of the inflection point temperature.

Matters are more complicated, since in reality char particles do not burn uniformly, due to the oxygen concentration gradient within the char particle. Equation (3) is still valid, but for obtaining the carbon mass flux the integration of a radius dependent preexponential reactivity constant is required. Just as in the case of uniform combustion, the increase of this factor with radius and time leads to a growth of conversion in the kinetic and internal transport limited regime and, again, consequently to a decrease of the inflection point temperature. The initial conditions for an exact, numerical evaluation are still given by the equations derived in Sections 3 and 4.

From these considerations it is clear why the "Progressive Conversion Model"[8], which starts from Eq. (3) but does not take time dependences into account, cannot be a proper model for fluidized bed combustion.

The remaining question is whether the ignition mode is critical or noncritical. By means of the model drawn up we are able to determine the
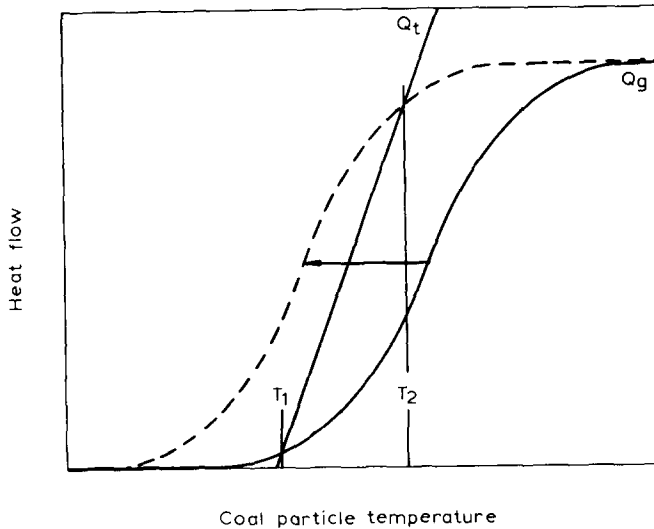
Fig. 11. Illustration of the mechanism causing char-ignition delay in fluidized bed combustors.

situation at the beginning of ignition and to formulate an expectation of the further development. For a certain char type and oxygen molfraction Figs. 9 and 10 show that the initial circumstances are noncritical, since for all bed temperatures the inclination of heat transfer is steeper than that of heat generation. The influence of the initial char particle size is made explicit in Fig. 12. In the diameter range from 3 to 15 mm the ratio of the inclinations of heat generation and transfer is unaffected by this diameter.

Since oxygen mol-fraction variations from 0.04 to 0.21 are demonstrated in fluidized bed combustors [14], ignition in oxygen lean zones is likely. The meaning of this mol fraction for the initial condition is shown in Fig. 13. It remains noncritical, while the ratio of the two inclinations may increase up to a factor of 25.

An important reactivity parameter is the activation energy. For most char types its value lies between 50×10^6 and 320×10^6 J/kmol [8]. So, since our calculations are based on an activation energy of 140×10^6 J/kmol, and the maximum inclination of the heat generation curve is inversely proportional to it, this inclination can be twice as steep as calculated. Still, initial conditions are noncritical. In our approach the type of char is not only defined by activation energy but also by specific mass, the preexponential reactivity con-

stant, and internal diffusivity. The influence of the latter parameters, however, were not investigated in this study.

Equation (15d) shows that the decrease of the inflection point temperature causes an increase of the inflection point inclination. It seems possible that, though starting as a noncritical process, ignition becomes critical. We present arguments why during the whole ignition period, circumstances remain noncritical. The most unfavorable starting position for this thesis is at the lowest bed temperature at which ignition of the considered char type was observed, which is 825K. For uniform combustion the argument is easy. Let us assume that the inflection point temperature shifts to 825K. For an 8 mm char particle and 21% oxygen (the original inflection point temperature is 1090K—cf. Fig. 7), Eq. (15d) yields that the maximum inclination of heat generation increases by a factor

$$(T_0^*/T_i^*)^2 = (1090/825)^2 = 1.75,$$

which is too small for the ignition process to become critical.

In the more realistic case of nonuniform combustion Eqs. (15) are not simply applicable, but must be adjusted. Instead of Eq. (9), we postulate a time dependent solution for the effectiveness
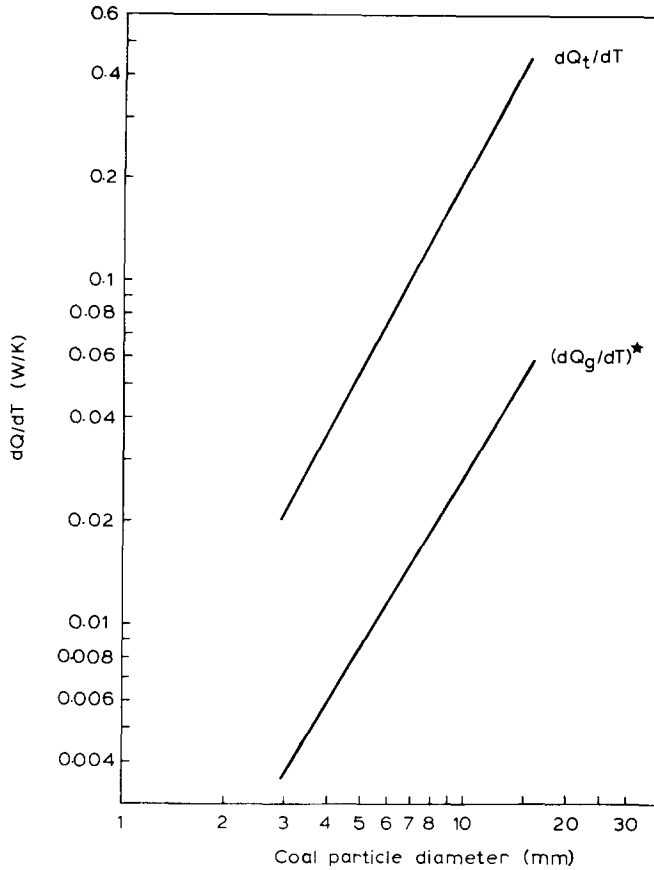
Fig. 12. Inclination of the heat transfer curve and heat generation curve at its inflection point as functions of char particle diameter. $X_{O_2} = 0.21$, $T_b = 1073K$.

factor,

$$\eta = C(t)(3/\phi)[(\phi - \tanh \phi)/\tanh \phi], \qquad (16)$$

on the understanding that the Thiele modulus is still defined by the initial values of the parameters in Eq. (8) and where $C(t)$ depends on the char burn-off history and therefore on time. The char burn-off history factor $C(t)$ may depend on bed temperature and initial char particle size. At $t = 0$, $C(t) = 1$ to make this solution compatible with the solution given in Eq. (9). Thus it is assumed that the temperature dependence of the effectiveness factor remains the same during the ignition period. In a procedure analogous to the derivation of Eqs. (14) and (15) we now find

$$T^* \simeq (E/R)/\ln[C(t)^2\rho D_e A \Lambda_{O_2}/k^2] \qquad (17a)$$

and

$$(\partial Q_g/\partial T)^* \simeq \tfrac{1}{8} \pi d^2 (k/\Lambda_{O_2})(R/E)$$
$$\times \{\ln[C(t)^2\rho A \Lambda_{O_2}D_e/k^2]\}^2 C_b H_r \qquad (17b)$$

$$\simeq \tfrac{1}{8} \pi d^2(k/\Lambda_{O_2})(E/RT^{*2})C_b H_r, \qquad (17c)$$

where reactivity parameters are given by their initial values.

Equations (17c) and (15d) are identical, and therefore the same argument holds. The entire ignition process is noncritical. General validity of this thesis might be qualified by considering the influence of heat transfer by other bed materials.
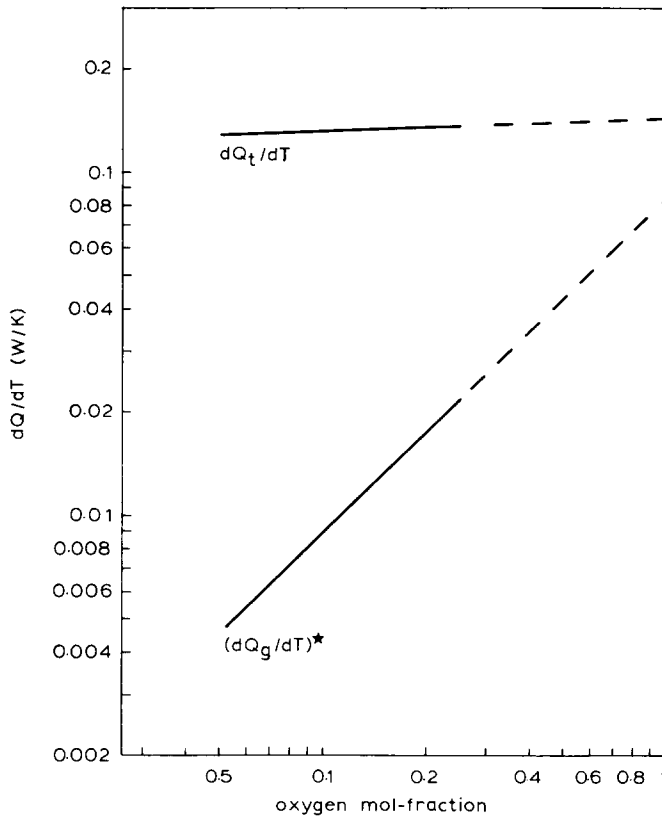
Fig. 13. Inclination of the heat transfer curve and heat generation curve at its inflection point as functions of the oxygen mol-fraction. ———, calculated; - - -, extrapolated. d = 8 mm, T_b = 1073K.

6. CONSEQUENCES AND POSSIBILITIES FOR FUTURE RESEARCH

An important question for practical purposes is, How long does it take for newly introduced coal particles to attain an overtemperature which is sufficiently high to maintain or start up combustion? The temperature needed depends on the combustor's heat losses and will not be determined here. Theoretically, the question posed is, How fast and how far does the inflection point temperature of the heat generation curve decrease during ignition? We are unable to answer this question here, because the char burn-off history factor $C(t)$, introduced in Eqs. (16) and (17), is not yet known.

An attempt was made to measure the ignition delay by means of a transparent fluidized scale

model and visual observation of the char particle [1-3]. But, since fluidized bed ignition appears to be a noncritical process without Semenov Jump, the moment of visible glowing cannot be an objective criterion. Still, this has drawn attention to the phenomenon of ignition delay and the importance of bed temperature.

Essentially there are two possibilities for future research. One is to make char particle temperatures measurable—for instance, by means of a freely moving thermocouple—and to record the temperature history. The other is to design a device with mass transfer similar to those in fluidized beds, but with poor heat transfer properties, in order to attain a critical ignition condition. Visual observation of the Semenov Jump will yield a good indication of the changes in heat generation. Values presented in Fig. 9 may serve as an

indication of upper limits of heat transfer in such a device. The conical quartz tube, as used by Ragland et al. [21] may be developed further to fit these constraints.

APPENDIX

Heating Times

The energy balance for a spherical layer within the char particle reads

$$(H_r/C_p M_C) A \, \exp(-E/RT) \, C^m$$

$$= \frac{\partial T}{\partial t} - \frac{1}{r^2} \frac{\partial}{\partial r} \left(r^2 \frac{\lambda}{\rho C_p} \frac{\partial T}{\partial r} \right) \qquad (18)$$

with the boundary conditions

$r = 0$: $\partial T/\partial r = 0$, $T = T_c$

$r = d/2$: $\partial T/\partial r = (\alpha/\lambda)(T_b - T_s)$, $T = T_s$.

For nonreacting spheres heating up to the bed temperature Eq. (18) reduces to

$$\partial T/\partial t = \frac{1}{r^2} \frac{\partial}{\partial r} \left(r^2 \frac{\lambda}{\rho C_p} \frac{\partial T}{\partial r} \right) . \qquad (19)$$

This equation is used to estimate the heating times of char particles to reach the bed temperature, shown in Fig. 3. It is clear that the temperature rise of reacting spheres is faster than that of nonreacting spheres. These estimations, therefore, provide upper values. For constant thermal diffusivity $\lambda/\rho C_p$, Eq. (19) has been analytically solved and given as function of Biot and Fourier numbers [15]. Though the thermal diffusivity of char rises

with increasing temperature, as may be inferred from Refs. [16] and [17], these solutions may still be of use to our purpose.

The calculated heating times are defined by the the time required for a 90% reduction of the original driving force: $(T_b - T_c)/(T_b - T_0) = 0.1$. Results as well as necessary data and their sources are listed in Table 3.

Isothermal Ignition

In this paper it is assumed that the char particle is isothermal. We shall show here why this is allowed.

From Eqs. (3) and (18) it follows that

$$-\frac{1}{r^2} \frac{\partial}{\partial r} \left(r^2 \frac{\lambda}{\rho C_p} \frac{\partial T}{\partial r} \right) + \frac{\partial T}{\partial t}$$

$$= (1/M_C) \left\{ \frac{1}{r^2} \frac{\partial}{\partial r} \left[(r^2 D_e H_r/\lambda C_p \Lambda_{O_2}) \frac{\partial C}{\partial r} \right] \right.$$

$$\left. - (H_r/\rho C_p \Lambda_{O_2}) \frac{\partial C}{\partial t} \right\} .$$

Quasi-stationary integration yields

$$\frac{\partial T}{\partial r} = (H_r D_e/\lambda \Lambda_{O_2} M_C) \frac{\partial C}{\partial r} .$$

The integration constant is 0, due to the boundary conditions at $r = 0$. A second integration, making use of the boundary conditions, gives

$$T_s - T_c = -(H_r D_e/\lambda \Lambda_{O_2} M_C)(C_s - C_c),$$

which is maximum for $C_s = C_b$ and $C_c = 0$.

TABLE 3

Heating times for $(T_b - T_c)/(T_b - T_0) = 0.1$[a]

T_b(K)	C_p(J/kg K)	λ(W/m K)	α(W/m² K)	Bi	Fo	t(s)
1100	2850	1.17	685	2.34	0.63	25
1000	2600	0.83	645	3.11	0.56	28
900	2350	0.49	600	4.90	0.46	35
800	2100	0.19	550	1.83	0.38	69

[a] $d = 8$mm; C_p and λ after Refs. [16] and [17] and evaluated at $T = (T_c + T_b)/2$.

Therefore,

$$(T_c - T_s)_{max} = (H_r D_e / \lambda \Lambda_{O_2} M_C) C_b$$

$$= (H_r D_e / \lambda \Lambda_{O_2} M_C)(X_{O_2} P M_{O_2} / R T_b).$$

Again, maximum temperature differences exist for low bed temperatures, maximum oxygen mol-fraction, and conversion to CO_2 rather than CO. So we take T_b = 825K (the lowest bed temperature where char ignition was observed), X_{O_2} = 0.21, and z = 0. For atmospheric pressure we find $(T_c - T_s)_{max}$ = 0.7K, which has no influence on reactivity in the considered temperature range.

This result is obtained on the condition that the process is quasi-stationary, i.e., that

$$\frac{1}{r^2} \frac{\partial}{\partial r} \left(r^2 \lambda \frac{\partial T}{\partial r} \right) \gg \rho C_p \frac{\partial T}{\partial t}$$

and

$$\frac{1}{r^2} \frac{\partial}{\partial r} \left(r^2 D_e \frac{\partial C}{\partial r} \right) \ll \frac{\partial C}{\partial t}.$$

The moment at which these conditions are satisfied must be established experimentally. We expect that this moment will be attained after the period of rapid heating up to about the bed temperature.

SYMBOLS

A preexponential reactivity constant, $(kg/m^3)^{-m}/s$

Ar $g d_b^3 \rho_b / \rho_g \nu_g$, Archimedes number, dimensionless

C oxygen concentration, kg/m^3

$C(t)$ char burn-off history factor, dimensionless

C_p specific heat of char, J/kg K

D_b binary diffusivity, m^2/s

D_e effective diffusivity, m^2/s

D_K Knudsen diffusivity, m^2/s

d char particle diameter, m

d_b bed particle diameter, m

E activation energy, J/kmol

g gravity constant, s/m^2

H_j formation enthalpy of species j from the elements, J/kmol

H_r reaction enthalpy per mole of carbon, J/kmol

h_j specific enthalpy of species j, J/kg

k external mass transfer coefficient, m/s

M molecular mass, kg/kmol

m char particle mass, kg
reaction order, dimensionless

$\dot{m}_j$ mass flow of species j, kg/s

Nu_{max} $\alpha_{max} d_b / \lambda_g$, maximum Nusselt number, dimensionless

Q_g heat flow generated by the char particle, J/s

P pressure, N/m^2

R universal gas constant, J/kmol K

Re $d U_f / \nu_g$, Reynolds number, dimensionless

R_m reactivity on actual mass base (carbon mass flow/mass of actual present char), s^{-1}

r radius, m

T char particle temperature, K

t time, s

U internal energy of the char particle, J

U_f fluidization velocity, m/s

U_{mf} minimum fluidization velocity, m/s

X mol-fraction, dimensionless

z ratio of CO and CO_2 production, kmol CO/kmol CO_2

Greek Symbols

α heat transfer coefficient, $J/s K m^2$

Λ_j gravimetric conversion coefficient for the formation of species j (mass flow of species j/total carbon mass flow), dimensionless

δ pore diameter, m

ϵ bed porosity, dimensionless

η effectiveness factor, dimensionless

ϕ Thiele modulus, dimensionless

ν viscosity, m^2/s

λ thermal conductivity, J/s K m

ψ char porosity, dimensionless

ρ specific mass, kg/m^3

Indices

b bed particle, bulk of the bed

C carbon

c char particle center

e effective
f fluidization
g generation, fluidizing gas
i ignition time
j species j
max maximum
mf minimum fluidization
O oxygen
p char particle, constant pressure
r reaction
s char particle surface
t transfer
* inflection point
0 $t = 0$

REFERENCES

1. Radovanović, M. Prins, W., and Siemons, R. V., *Symposium on the Use of Lignites in Thermoenergetics* (in Yugoslavian), Masinski Fakultet, Belgrade, 1983, pp. 93–102.
2. Prins, W., Fluidized Bed Combustion of a Single Carbon Particle, Ph.D. thesis, University of Twente, Enschede, 1987, Ch. 1.
3. Radovanović, M., in *Advanced Course on Fluidized Bed Combustion, Dubrovnik 1984* (M. Radovanović, Ed.), Twente University of Technology (Dept. Mech. Eng), 1984, Ch. 5.
4. Essenhigh, R. H., in *Chemistry of Coal Utilization* (M. A. Elliot, Ed.), New York, 1981, 2nd Suppl. Vol., pp. 1285–1297.
5. Vulis, L. A., *Thermal Regimes of Combustion*, McGraw-Hill, New York, 1961.
6. Aris, R., *Chem. Engng. Sci.* 6:262–268 (1957).
7. Mehta, B. N. and Aris, R., *Chem. Engng. Sci.* 26:1699–1712 (1971).
8. Leaurendeau, N., *Prog. Energy Combust. Sci.* 4:211–270 (1978).
9. Prins, W., Casteleyn, T. P., Draijer, W., and Van Swaaij, W. P. M., *Chem. Engng. Sci.* 40:481–497 (1985).
10. Bliek, A., Dissertation, Twente University of Technology, Enschede, 1984.
11. Arthur, J. R., *Trans. Faraday Soc.* 47:164–178 (1951).
12. Rossberg, M., and Wicke, E., *Chemie-Ing.-Techn.* 28:181–189 (1956).
13. Prins, W., Draijer, W., and Van Swaaij, W. P. M., *16th ICHMT Symposium* (W. P. M. van Swaaij and N. H.Afgan, Eds.), Hemisphere, Washington, 1986, pp. 317–331.
14. Sinha, P. K., Datta, A. B., Nandi, S. S., and Bhaduri, D., *Fuel* 59:527–531 (1980).
15. Heisler, M. P., *Trans. ASME* 69:227–236 (1947).
16. Badzioch, S., Gregory, D. R., and Field, M. A., *Fuel* 43:267–280 (1964).
17. Melchior, E., and Luther, H., *Erdöl Kohle Erdgas Petrochemie* 28:379–385 (1975).
18. Landolt-Börnstein, *Zahlenwerte und Funktionen aus Physik, Chemie, Astronomie, Geophysik und Technik,* Springer Verlag, Berlin, 1955.
19. Weast, R. C. (Ed.), *C.R.C. Handbook of Chemistry and Physics* 63rd Ed., Boca Raton, 1982.
20. *Dubbel's Taschenbuch für den Maschinenbau,* Berlin, 1966.
21. Ragland, K. W., Jehn, T. C., and Yang, J. T., *18th Symposium (International) on Combustion,* The Combustion Institute, 1981, pp. 1295–1303.